Physics of Fluids

# Circular turbulent wall jets in quiescent and coflowing surroundings

Cite as: Phys. Fluids **34**, 025116 (2022); https://doi.org/10.1063/5.0079921
Submitted: 25 November 2021 • Accepted: 17 January 2022 • Published Online: 10 February 2022

**Mohammad Kazemi, Babak Khorsandi and Laurent Mydlarski**

Physics of Fluids ARTICLE scitation.org/journal/phf

# Circular turbulent wall jets in quiescent and coflowing surroundings

Cite as: Phys. Fluids **34**, 025116 (2022); doi: 10.1063/5.0079921
Submitted: 25 November 2021 · Accepted: 17 January 2022 ·
Published Online: 10 February 2022



Mohammad Kazemi,[1] Babak Khorsandi,[1,a)] and Laurent Mydlarski[2]

## AFFILIATIONS

[1]Department of Civil and Environmental Engineering, Amirkabir University of Technology (Tehran Polytechnic), 350 Hafez Avenue, Tehran, 159163-4311, Iran
[2]Department of Mechanical Engineering, McGill University, 817 Sherbrooke Street West, Montréal, Quebec H3A 0C3, Canada

[a)]Author to whom correspondence should be addressed: b.khorsandi@aut.ac.ir

## ABSTRACT

The dynamics and mixing of circular turbulent wall jets released into both a quiescent background and coflowing stream have been investigated experimentally. The statistics of the velocity field (measured by way of acoustic Doppler velocimetry) for the wall jets emitted into a quiescent background agree well with those of the other studies. The experiments involving coflowing wall jets were undertaken at three different jet-to-coflow velocity ratios. The coflowing wall jets were found to decay and spread at slower rates and have lower mean lateral velocities compared to wall jets in quiescent surroundings. Moreover, the decay and spreading rates of the coflowing wall jets increased with increasing jet-to-coflow velocity ratios. The wall jets issued into a coflow also developed more slowly and reached self-similarity at farther downstream distances relative to those emitted into a quiescent background. Given the decreased decay rate, spreading rate, and mean lateral velocities of wall jets in the presence of a coflow, it was inferred that the entrainment into, and mixing of, the wall jets was reduced, presumably due to the suppresion by the coflow of the vortical structures that characterize wall jets in quiescent backgrounds. Finally, the root-mean-square velocities of the wall jets increased when a coflow was present, and were found to be nearly self-similar in the range of measurements studied herein, in contrast with coflowing jets (that are not released in the vicinity of a wall).



## I. INTRODUCTION

A three-dimensional wall jet consists of a jet discharged from a nozzle, parallel to and along a nearby planar wall. Three-dimensional turbulent wall jets have attracted the attention of researchers due to their diverse engineering applications, as well as the interesting physical interaction between the jet and the near-wall flow. Examples of practical applications of turbulent wall jets include sewage outfalls in the ocean (Zhang *et al.*, 2018), capping underwater waste material in marine environments (Azimi *et al.*, 2014; Azimi *et al.*, 2015), film cooling of gas turbine blades and combustion chambers (Sharma *et al.*, 2019; Chokhar *et al.*, 2021), and airfoil boundary layer and drag control (Ji *et al.*, 2021; Xu *et al.*, 2021).

In the environmental and industrial applications of wall jets, the ambient fluid is rarely quiescent and its velocity is generally lower than that of the jet. However, almost all previous studies of wall jets only considered those in which the jet was released into stagnant surroundings. Yet, the presence of the ambient flow can influence the dynamics and mixing of wall jets. Moreover, the main direction of ambient flow may vary with respect to the jet axis. If the flow of the ambient fluid is parallel to the jet axis and flowing in the same direction, the flow is called a coflow. Coflowing circular wall jets are the subject of the present work.

Over the last five decades, the dynamics of three-dimensional wall jets released from circular or rectangular nozzles/pipes have been the subject of multiple studies, including those of Sforza and Herbst (1970), Launder and Rodi (1983), Padmanabham and Lakshmana Gowa (1991), Davis and Winarto (1980), Law and Herlina (2002), Sun and Ewing (2002), Agelin-Chaab and Tachie (2011), Shojaeizadeh *et al.* (2018), and Godi *et al.* (2019). Note that offset jets (e.g., Nyantekyi-Kwakye *et al.*, 2015; Dey *et al.*, 2017; Li and Huai, 2020) are similar to wall jets and have also been the subject of recent research. However, in the interest of both brevity and relevance to the present work, the rest of this section only focuses on wall jets released from circular nozzles/pipes.

The velocity field of wall jets is typically subdivided into two regions, known as the inner and outer layers (Agelin-Chaab and Tachie, 2011). The inner layer extends from the wall up to the point of maximum mean velocity, and the outer layer extends from this point

to the one at which the velocity asymptotes to that of the ambient fluid. The inner layer has characteristics of a boundary layer, whereas the outer layer resembles a (free) jet. It has been observed that the mean velocity and mean scalar concentration of circular wall jets are self-similar (Davis and Winarto, 1980; Law and Herlina, 2002; Agelin-Chaab and Tachie, 2011; Kakka and Anupindi, 2021). Agelin-Chaab and Tachie (2011) furthermore demonstrated that the Reynolds stresses become self-similar at distances farther downstream than those at which the mean velocities reach self-similarity. In the self-similar region, the lateral and vertical half-widths of circular wall jets have been shown to grow linearly with the downstream distance (Law and Herlina, 2002). It has also been observed that the lateral spreading rate in fully developed circular wall jets is several times greater than the vertical spreading rate, resulting in a very elongated jet cross section (i.e., the lateral dimension of the jet is much greater than that in the vertical dimension; Davis and Winarto, 1980). The larger lateral jet spreading rate is mainly caused by a secondary vortex that directs the flow toward the wall and then laterally away from the centerline (Launder and Rodi, 1983; Abrahamsson *et al.*, 1997; Law and Herlina, 2002). Furthermore, Law and Herlina (2002) emphasized the role played by the secondary vortex in the mixing of wall jets. The effect of Reynolds number and the jet's exit velocity profile were examined by Sun and Ewing (2002) for circular wall jets. While the development of the wall jet was not significantly influenced by changes in jet Reynolds numbers (for relatively high Reynolds numbers greater than 65 000), the jet exit velocity profile was found to affect the maximum axial velocity and the half-width of the jet.

The velocity field of circular wall jets in counterflow was also investigated by Mahmoudi and Fleck (2017). The dynamics of a wall jet in counterflow was found to be similar to those of a wall jet in a quiescent fluid near the jet exit, whereas farther downstream, where the relative magnitude of the counterflow's velocity (with respect to the jet velocity) increased, the wall jet structure was found to be significantly disrupted. It was shown that the maximum velocity decay rate and spreading rates were similar to those reported for a wall jet in a quiescent background for up to 70% of the penetration length (i.e., the downstream distance between the jet exit and the stagnation point). Beyond this location, they observed the velocity to decay linearly with downstream position and the jet width to rapidly increase. Profiles of the mean velocity and Reynolds stresses were also found to be self-similar within the range of downstream distances that correspond to 25%–80% and 30%–70% of the penetration length, respectively. Beyond that range, the Reynolds stresses drastically increased, and were no longer self-similar. Moreover, it was observed that the counterflow strengthened the vortical structures which enhance wall jet mixing.

Circular turbulent jets released (far from boundaries) into coflows have been the subject of numerous studies. It has been shown that the evolution of the mean velocities and mean scalar concentrations are self-similar (Antonia and Bilger, 1973; Nickels and Perry, 1996). However, unlike jets in quiescent backgrounds (free jets), the Reynolds stresses were not found to be self-similar (Antonia and Bilger, 1973; Smith and Hughes, 1977; Moeini *et al.*, 2021) and the widths of the velocity and concentration fields vary nonlinearly with downstream distance in coflowing jets (Chu *et al.*, 1999). Moreover, it stands to reason that the presence of a boundary adjacent to a coflowing jet will significantly alter its flow features.

Thus, ambient flow may have a considerable influence on the dynamics of circular wall jets and any result obtained from studies of circular wall jets in a quiescent background is unlikely to be applicable to coflowing circular wall jets. To the authors' knowledge, the effect of coflow on the dynamics of circular wall jets has not been previously studied. Therefore, the aim of the present work is to experimentally investigate the dynamics and mixing of circular turbulent wall jets released into a coflowing stream by way of simultaneous measurements of the three components of the velocity field. To this end, velocity statistics pertaining to circular wall jets emitted into a (i) quiescent background and (ii) coflow (with three different jet-to-coflow velocity ratios) will be reported. Specifically, the mean and the root-mean-square (RMS) velocities, mean velocity decay and spreading rates, and velocity spectra are presented and discussed.

The rest of this paper is structured as follows. The experimental apparatus and measurement techniques are described in Sec. II. The experimental results and discussion of circular wall jets released into a quiescent background and coflow are then presented in Sec. III. Finally, conclusions are drawn in Sec. IV.

## II. EXPERIMENTAL APPARATUS AND PROCEDURE

The experiments were undertaken in a closed-loop flume filled with water. As previously noted, the experiments were conducted in both a quiescent background and a coflowing stream. Figure 1 provides a schematic diagram of the setup. The 6-m-long flume had a $0.5 \times 0.5$ m$^2$ cross section and the water depth was maintained at 0.45 m for wall jets released into both a quiescent background and coflow. The walls and bottom of the flume were made of transparent glass. For the experiments investigating the wall jet in a quiescent background, the excess mass from the jet overflowed a 0.45-m-high weir at the end of the flume, which kept the water depth constant. For the wall jet experiments in a coflow, the water flowed from an upstream basin to the flume, and then flowed over a (shorter) 0.40-m-high weir into a downstream stilling basin. The water was then pumped from the downstream basin back to the upstream basin through a pipe. The upstream basin was connected to the flume by a curved symmetric contraction, which resulted in an approximately uniform flow into the flume. To improve the homogeneity and uniformity of the flow, the water passed through a perforated steel plate and a number of wooden-fiber blankets in the upstream basin (not shown in Fig. 1), and then an aluminum honeycomb positioned at the entrance to the flume's test section.

The jet consisted of an L-shaped brass pipe of 0.01-m inner diameter ($D$) mounted on a traversing mechanism. The pipe extended vertically for 0.9 m, of which the lower 0.45 m was submerged in the water. At 0.45 m below the water's surface, a 90° bend caused the jet to extend horizontally for 0.2 m before its exit, ensuring that the flow was fully developed at the exit of the pipe. Note that, for the coflowing wall jet experiments, the velocity deficit caused by the vertical jet pipe was a small percentage ($<1.5\%$) of the jet exit velocity and therefore not expected to affect the flow. The circular turbulent wall jet was discharged from the pipe in the downstream direction of the flume. The center of the jet exit was located 0.01 m above the bottom wall (i.e., $h/D = 1$, where $h$ is the distance from the center of the jet exit to the wall), 0.25 m from either sidewall, and 1.4 m from the start of the flume's test section. The measurements were conducted over the range $30 \leq x/D \leq 100$, where $x$ is the distance from the jet exit. The jet was

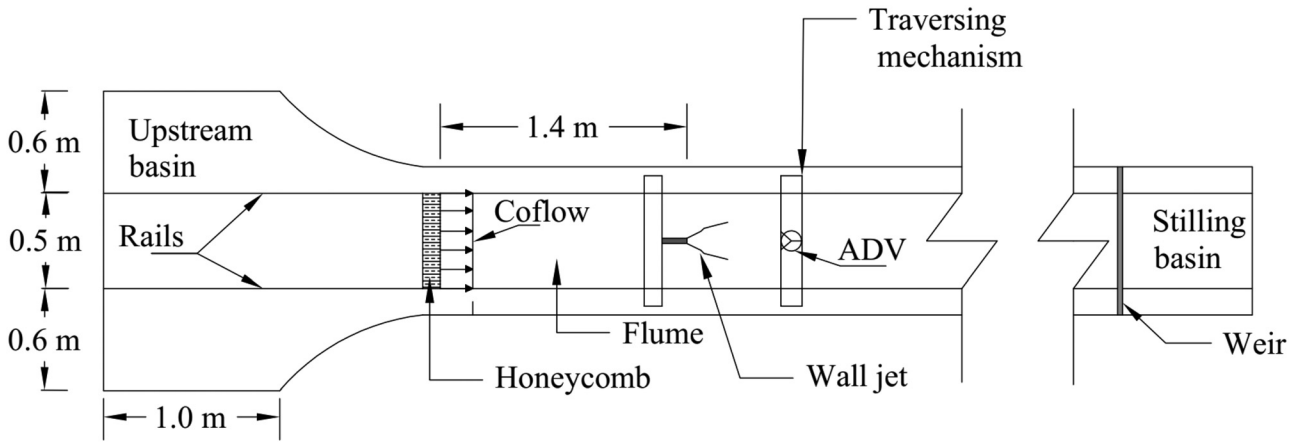


**FIG. 1.** Schematic of the top view of the flume, including the jet, acoustic Doppler velocimeter (ADV), and traversing mechanism (not to scale).

fed from a 0.1 $m^3$-constant head-reservoir, which was situated 3 m above the ground and was supplied with water from the stilling basin. The reservoir was connected by a plastic tube to the pipe that formed the jet. The flow rate was controlled by a ball valve and was measured using a Georg Fischer d32 DN 25 (Schaffhausen, Switzerland) flowmeter positioned downstream of the valve. The jet was discharged into a quiescent background with a Reynolds number ($\mathrm{Re} = U_j D/\nu$) of 10,000, where $U_j$ is the average wall jet exit velocity, and $\nu$ is the kinematic viscosity of water at 20 °C. In the present work, the coflowing wall jets had Reynolds numbers of 7000, 10 000, and 12 500.

A Nortek 10-MHz ADVLab (Rud, Norway) acoustic Doppler velocimeter (ADV) was used to measure the velocity field. The *x*-, *y*-, and *z*-directions of the ADV probe were aligned with the axial (*u* velocity), lateral (*v* velocity), and vertical (*w* velocity) directions of the wall jet, respectively. The sampling frequency was set to 25 Hz (the maximum). The ADV sampling volume is located 5 cm below its transmitter (Nortek, 2018), and this distance minimizes any flow disturbance by the probe (Khorsandi *et al.*, 2012). The maximum sampling volume height of 9.1 mm was used, resulting in minimal Doppler noise during measurements. As the integral length scale of the flow was much larger than the sampling volume dimensions in the range of measurements investigated herein, the spatial resolution is expected to be sufficient, especially for the large-scale measurements of the turbulence such as RMS velocities. (For more details, the reader is referred to Kazemi *et al.*, 2021.) Talcum powder was added to the water to increase the signal-to-noise ratio of the measurements (Moeini *et al.*, 2020). The ADV velocity range was set to span the full range of measured velocities. Data were recorded for 40 min (60 000 data points) for each test, which ensured convergence of the statistics. The output data were postprocessed using the phase-space thresholding method (Goring and Nikora, 2002; modified by Wahl, 2003), which is implemented in the WinADV software. The method was very effective in improving the data quality for the near-wall measurements.

## III. RESULTS AND DISCUSSION

This section presents the statistics of the velocity field of the wall jet issued into a quiescent surrounding as well as a coflowing stream. The former also serves as a validation of the measurements.

Figure 2 sketches the schematic of a wall jet velocity profile. In this figure, $U_m$ is the maximum axial (or streamwise) mean velocity; $z_m$ is the wall normal location of $U_m$; and $y_{1/2}$ and $z_{1/2}$ are the lateral and vertical positions, respectively, at which the velocity falls to $^1/_2 U_m$. Note that the *x*-, *y*-, and *z*-directions are referred to as axial, lateral, and vertical directions, and the velocity profiles in the lateral and vertical directions are measured in a *x*-*y* plane with $z = z_m$ and in a *x*-*z* plane with $y = 0$, respectively.

### A. Turbulent wall jet in a quiescent background

The ADV measurements were first taken in the flow generated by a circular turbulent wall jet at Re = 10 000 released into a quiescent background. The results are compared with prior studies of wall jets, including the hot-wire anemometry (HWA) measurements of Davis and Winarto (1980) (abbreviated in our figures as DW), the HWA measurements of Abrahamsson *et al.* (1997) (AJL), the particle image velocimetry (PIV) measurements of Law and Herlina (2002) (LH), the HWA measurements of Sun and Ewing (2002) (SE), and the PIV measurements of Agelin-Chaab and Tachie (2011) (AT). The ADV measurements of a free circular jet undertaken in the same setup (Kazemi *et al.*, 2021) (KKM), but away from the wall, are also presented for comparison.

Table I presents a summary of results from the past and present studies of circular turbulent wall jets released into quiescent backgrounds. The decay rate ($n$) refers to the power-law decay exponent of the maximum axial mean velocity [$\frac{U_m}{U_j} = A\left(\frac{x}{D}\right)^{-n}$, where $A$ is a constant]. Due to the presence of the wall, the decay rate of the wall jet is higher than that of a free jet ($n \sim 1$). The spreading rate is defined as the downstream growth rate of the wall jet and is defined, in the *y*- and *z*-directions, by $S_y = \frac{dy_{1/2}}{dx}$ and $S_z = \frac{dz_{1/2}}{dx}$, respectively. $S_y$ and $S_z$ were, respectively, calculated by taking the derivative of curves fit to the values of $y_{1/2}$ and $z_{1/2}$ (obtained from velocity profiles) plotted as a function of the downstream distance. Compared to a free jet, wall jets grow at a higher rate in the lateral direction, but at a lower rate in the vertical one. It can be observed that there are variations in the decay and spreading rates among the results of various studies presented in the table. These differences may be due to different initial conditions

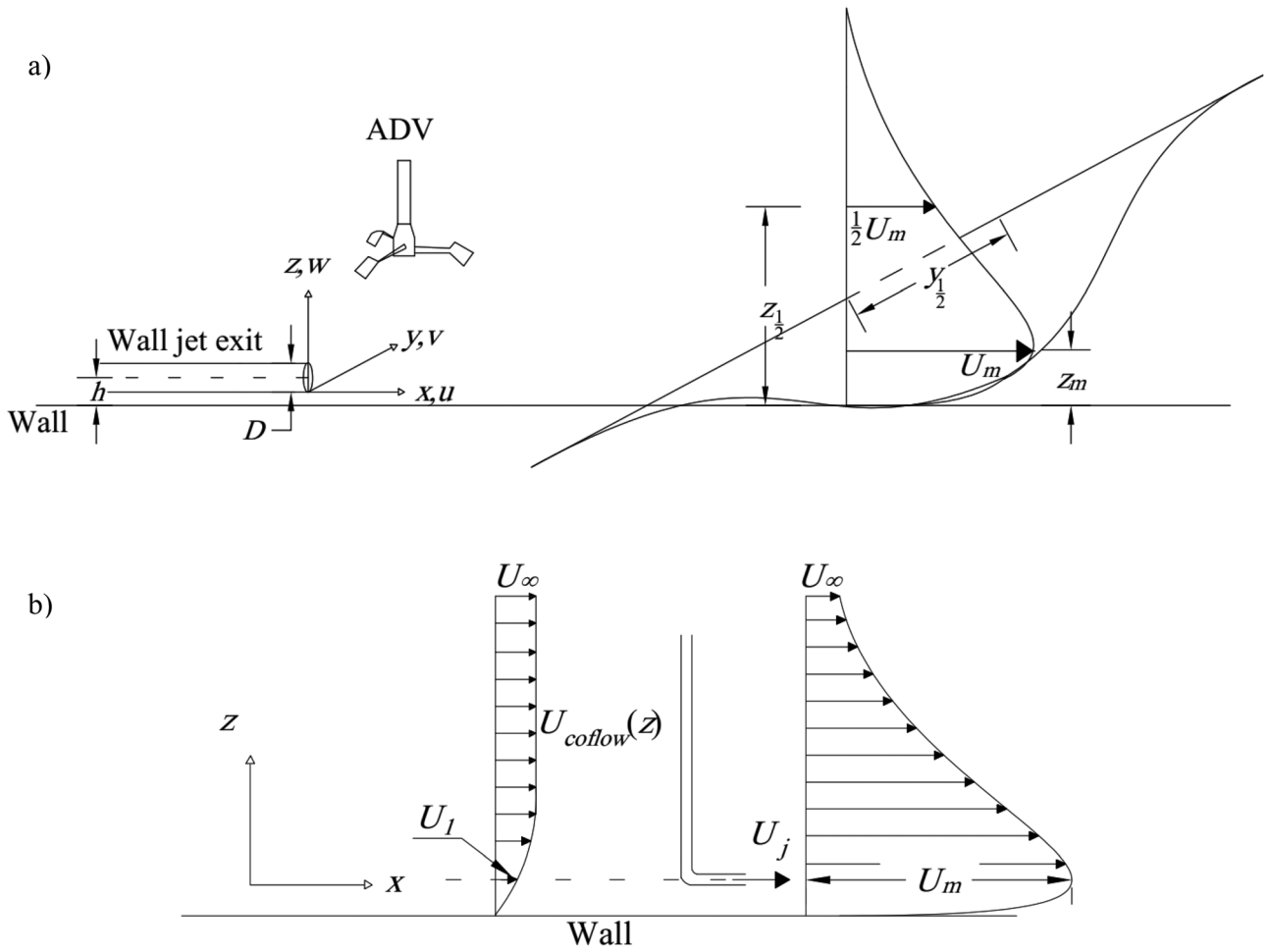


**FIG. 2.** Schematic of the velocity profiles of (a) the wall jet and ADV probe, and (b) the coflowing wall jet.

[i.e., the jet Reynolds numbers, outlet velocity profiles (Nejatipour and Khorsandi, 2021), and jet exit heights above the wall] as well as the size of the enclosure in which the experiments were conducted (Hussein *et al.*, 1994). Overall, the results of the present study are in good agreement with those of the past studies, falling within the ranges of the parameters observed within these studies.

Figures 3(a)–3(e) plot the profiles of the mean velocities of the wall jet at Re = 10 000 in the lateral and vertical directions. In Fig. 3(a), the profiles of the axial velocity of the wall jet in the lateral and vertical directions are compared to the (axisymmetric) velocity profile of a free, axisymmetric turbulent jet (at the same Reynolds number, also at $x/D = 30$). It can be observed that the wall jet profile in the lateral direction is wider, whereas the profile in the vertical direction is similar to that of the free jet. The axial velocity profiles measured at $x/D = 30$, 45, and 60 in the lateral and vertical directions are plotted in Figs. 3(b) and 3(c), respectively. The profiles at the different downstream positions collapse onto a single curve, indicating that the mean velocity is self-similar. There is also good agreement with the profiles measured in previous studies using other techniques and despite the different initial conditions. More scatter is observed in the profiles of the $V$ and $W$ velocities [Figs. 3(d) and 3(e), respectively] due to smaller magnitude of these velocities, which result in higher uncertainties. The self-similarity of the mean lateral and vertical velocities does not appear to hold at downstream distances $x/D < 45$. Note that the vertical mean velocities are negative, because the flow is toward the wall. This presumably arises due to secondary mean vortices (explained earlier), which direct the flow downward (Launder and Rodi, 1983; Abrahamsson *et al.*, 1997; Law and Herlina, 2002).

The lateral and vertical profiles of the RMS velocities of the wall jet at $x/D = 30$, 45, and 60 for Re = 10 000 are shown in Fig. 4. It can be seen that the data measured at different values of $x/D$ collapse, implying that the RMS velocities are self-similar for $x/D \geq 30$. The maximum values of the lateral RMS velocity profiles are located in the outer layer ($z > z_m$), consistent with the observation of Agelin-Chaab and Tachie (2011). The variations of the RMS velocity profiles in the different studies may, once again, be attributed to their different initial conditions. Note that the RMS velocity profiles measured in the present study lie within the range of those reported by the other researchers. The results presented in this section validate the accuracy of measurements in the wall jet even at points located very close to the wall.

**TABLE I.** Summary of present and previous research results on three-dimensional wall jets. CSW: cross single wire; SW: single wire; $h'$: distance normal to the plate from one edge of a circular orifice.

| Study | Circular outlet geometry, diameter and distance from wall | Velocity measurement technique | Measurement range | Reynolds number | $n$ $[U_m = A(x)^{-n}]$ | $\frac{dy_{1/2}}{dx}$ | $\frac{dz_{1/2}}{dx}$ | $\frac{dy_{1/2}}{dx}/\frac{dz_{1/2}}{dx}$ |
|---|---|---|---|---|---|---|---|---|
| Present study | Pipe<br>$D = 10$ mm<br>$h/D = 1$ | ADV | $30 \leq x/D \leq 110$ | 10 000 | 1.24 | 0.26 | 0.04 | 6.5 |
| Agelin-Chaab and Tachie (2011) | Pipe $D = 7$ mm<br>$h/D = 0.5$ | PIV | $30 \leq x/D \leq 60$ | 5000<br>10 000<br>20 000 | 1.15 | 0.25 | 0.05 | 4.7 |
| Law and Herlina (2002) | Orifice $D = 5.5$ mm<br>$h/D = 0.69$ | PIV | $0 \leq x/D \leq 50$ | 5500–13 700 | 1.07 | 0.21 | 0.04 | 5.0 |
| Sun and Ewing (2002) | Contraction nozzle<br>$D = 38.1$ mm | HWA | $0 \leq x/D \leq 90$ | 65 000<br>108 000 | 1.14 | 0.27 | 0.053 | 5.0 |
| Abrahamsson *et al.* (1997) | Contraction nozzle<br>$D = 20$ mm | HWA<br>CSW<br>SW | $50 \leq x/D \leq 90$ | 53 000–105 000 | 1.29 | 0.32 | 0.065 | 4.9 |
| Padmanabham and Lakshmana Gowda (1991) | Orifice segments<br>$h'/D$ | HWA | $0 \leq x/D \leq 100$ | 95 400 | | | | |
| | 1 | | | | 1.15 | 0.21 | 0.045 | 4.6 |
| | 0.8 | | | | 1.12 | 0.21 | 0.043 | 4.9 |
| | | | | | 1.15 | 0.24 | 0.049 | 4.9 |
| | 0.5 | | | | 1.12 | 0.25 | 0.040 | 6.2 |
| | 0.23 | | | | | | | |
| Davis and Winarto (1980) | Contraction nozzle<br>$h/D$ | HWA | $5 \leq x/D \leq 60$ | 170 000 | 1.15 | | | |
| | 1 | | | | | 0.32 | 0.037 | 8.6 |
| | 1.5 | | | | | 0.33 | 0.036 | 9.1 |
| | 2.5 | | | | | 0.29 | 0.039 | 7.4 |
| | 4.5 | | | | | 0.23 | 0.046 | 5 |
| Free jet (Kazemi *et al.*, 2021) | Pipe<br>$D = 10$ mm | ADV | $20 \leq x/D \leq 90$ | 10 000 | 1.0 | 0.10 | 0.10 | 1.0 |

## B. Circular turbulent wall jets issued into a coflowing stream

### 1. Coflow characteristics

The mean downstream velocity profiles of the coflow are depicted in Fig. 5. To this end, we define $U_\infty$ as the mean velocity at the center of the channel and $U_1$ as the mean velocity at $z = z_m$. Both $U_\infty$ and $U_1$ were measured along the lateral direction in the channel and their profiles are given in Figs. 5(a) and 5(b), respectively. $U_{coflow}$ (which is a function of $z$) was measured along the vertical direction at the mid-width of the channel, and its profile is given in Fig. 5(c). It can be seen that the mean velocities are approximately uniform in the lateral direction. The lack of symmetry in the respective profiles is presumably due to minor imperfections at the inlet of the flume (e.g., the contraction). The mean velocities become smaller as the wall is approached in the vertical direction (at approximately $z \leq 10$ cm), as expected. Given that the vertical width of the wall jet ($\sim 2z_{1/2}$) was less than 10 cm in the range of measurements, the wall jet was located in the bottom-wall boundary layer of the flume. Similar to their mean flow counterparts, $u_{\infty\ rms}$ and $u_{1\ rms}$ are the RMS velocities measured at the center of the channel and $z = z_m$, respectively, and their values are tabulated in Table II which presents the statistics of the coflow. The statistics were averaged over the range $30 \leq x/D \leq 100$, the interval in which the wall jet measurements were conducted.

### 2. Coflowing wall jets

The results pertaining to wall jets released into a coflowing stream are presented in this section. Three wall jets were issued into the coflow with Reynolds numbers of 7000, 10 000, and 12 500, respectively, corresponding to the nondimensional velocity excesses ($\lambda_j \equiv \frac{U_j - U_1}{U_1}$) of 24, 36, and 45. Note that this quantity was calculated based on $U_1$, as opposed to its calculation using $U_\infty$ for jets in a coflow without a wall. Using $U_\infty$ for the excess velocity

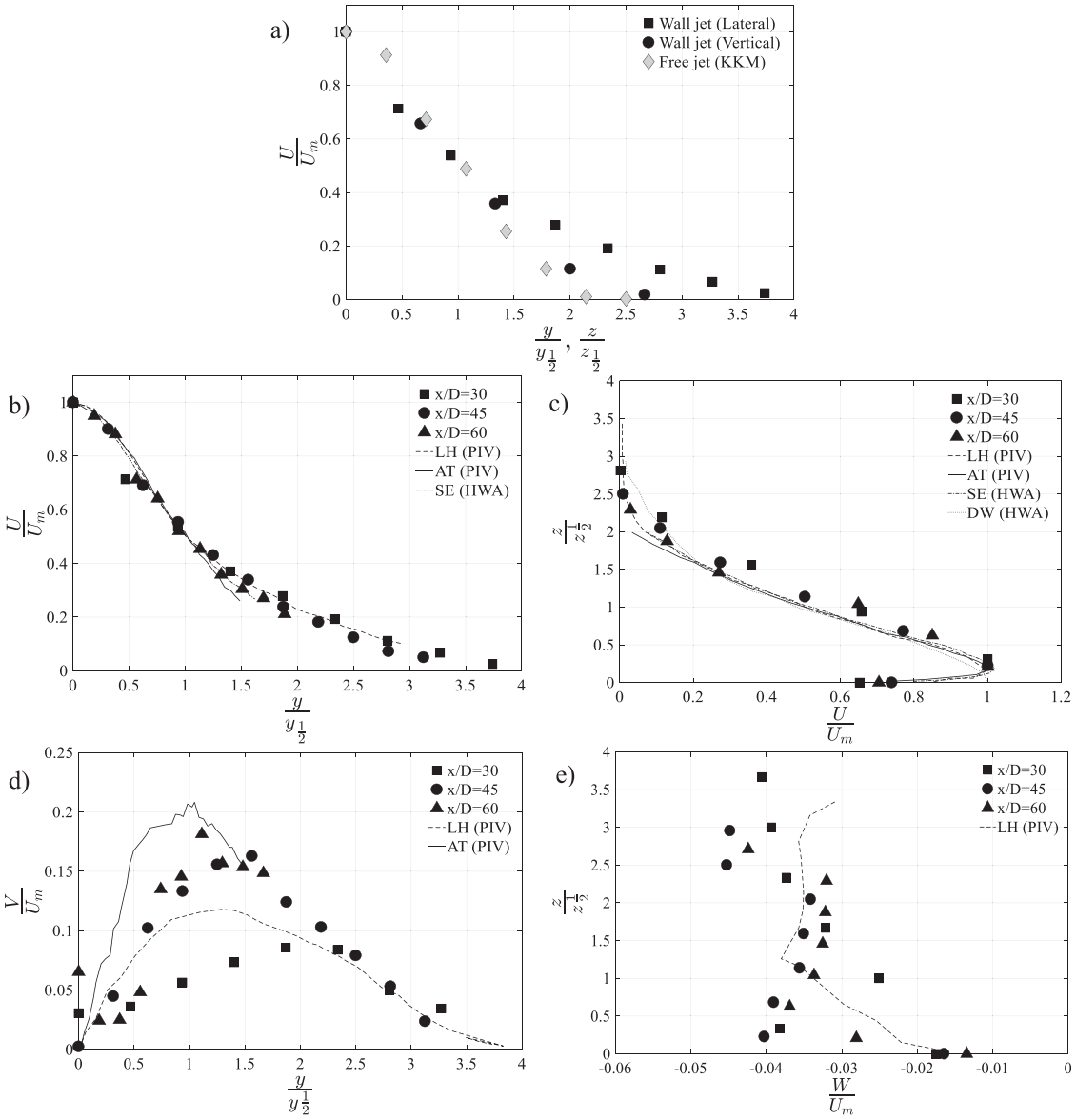


**FIG. 3.** Normalized profiles of the mean (a)–(c) axial, (d) lateral, and (e) vertical velocities of the circular wall jet released into a quiescent background and compared with results of other studies.

calculations would not be sensible as doing so would result in negative velocities in the profiles of coflowing wall jets, especially in the vicinity of the wall.

The downstream evolution of the maximum axial mean velocity excess, $U_{m_0}$ ($\equiv U_m - U_1$), normalized by the mean coflow velocity, for $\lambda_j = 24$, 36, and 45, is plotted in Fig. 6. The graphs are plotted as a function of $x/D$ in linear coordinates in Fig. 6(a), $x/l_m$ in linear coordinates in Fig. 6(b), and $x/l_m$ in log–log coordinates in Fig. 6(c). $l_m$ is the momentum length of the flow, defined as $l_m \equiv \frac{M_e^{1/2}}{U_1}$ (Nickels and Perry, 1996; Moeini *et al.*, 2021), where $M_e$ is the excess momentum of the wall jet and is assumed to be constant (Nickels and Perry, 1996).

As can be seen in Fig. 6(a), the mean velocity decays as the wall jets develop downstream. The data can be fit with power laws of the form $\frac{U_{m_0}}{U_1} = A_0 \left(\frac{x}{D}\right)^{-n_0}$, where $A_0$ is a constant and $n_0$ is the decay exponent. The decay exponents for various values of $\lambda_j$ are reported in Table III. It can be seen that the wall jet decays faster as $\lambda_j$ increases. Moreover, the wall jets in a coflow decay slower than the wall jet emitted into a quiescent background. It is reasonable to expect that the decay exponent of the coflowing wall jet tends to that of the wall jet in a quiescent background ($\sim$1.24) as $\lambda_j \to \infty$.

The maximum axial mean velocity excesses for wall jets with different values of $\lambda_j$ effectively collapse onto one curve when plotted as a

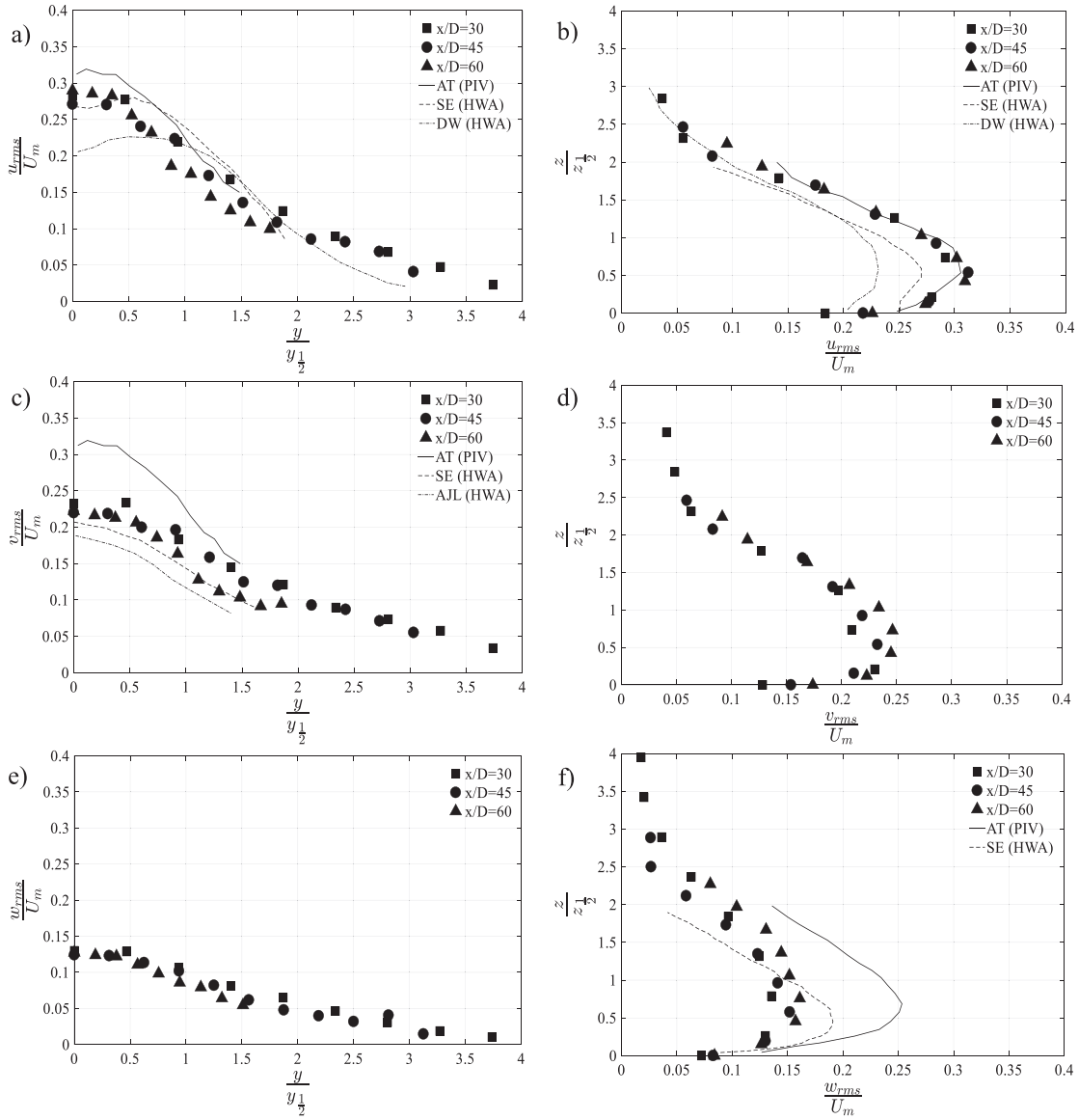


**FIG. 4.** Lateral and vertical profiles of the (a) and (b) axial, (c) and (d) lateral, and (e) and (f) vertical RMS velocities (normalized by the maximum axial mean velocity) of the wall jet released into quiescent background and compared with the results of other studies.

function of $x/l_m$ [Figs. 6(b) and 6(c)]. The small difference between the measurements for various $\lambda_j$ vanishes as the coflowing wall jets develop downstream. The collapse of the data indicates that the mean velocity excess is only a function of the nondimensionalized downstream distance and is independent of $\lambda_j$ for the range of $\lambda_j$ studied herein. The collapsed data has a decay exponent of 0.97, thus, coflowing wall jets may decay at a slightly slower rate compared to coflowing jets (that have a decay exponent of 1 for $x/l_m < 10$) (Nickels and Perry, 1996; Chu *et al.*, 1999; Or *et al.*, 2011; Moeini *et al.*, 2021).

Figure 7 depicts the lateral and vertical profiles of the normalized axial mean velocity excess plotted for various values of $\lambda_j$ for three downstream locations ($x/D = 30$, 60, and 80). It can be seen that, under the influence of the coflow, the mean velocity excess is nearly self-similar in both the lateral and vertical directions and is independent of $\lambda_j$ at each downstream location, consistent with the observations in Figs. 6(b) and 6(c). The self-similarity is slightly disrupted at the edges of the jet, where the mean velocities were low and probably disrupted by the coflowing stream.

The lateral and vertical profiles of the normalized axial mean velocity excess for $\lambda_j = 36$ at $x/D = 30$, 60, and 80 are compared with the self-similar profiles of a wall jet in a quiescent background in Fig. 8. The self-similarity of the mean velocity is delayed (compared to that of the wall jet in quiescent background) and holds for $x/D \geq 60$. Alternatively stated, it takes longer for wall jets to develop in a coflow.

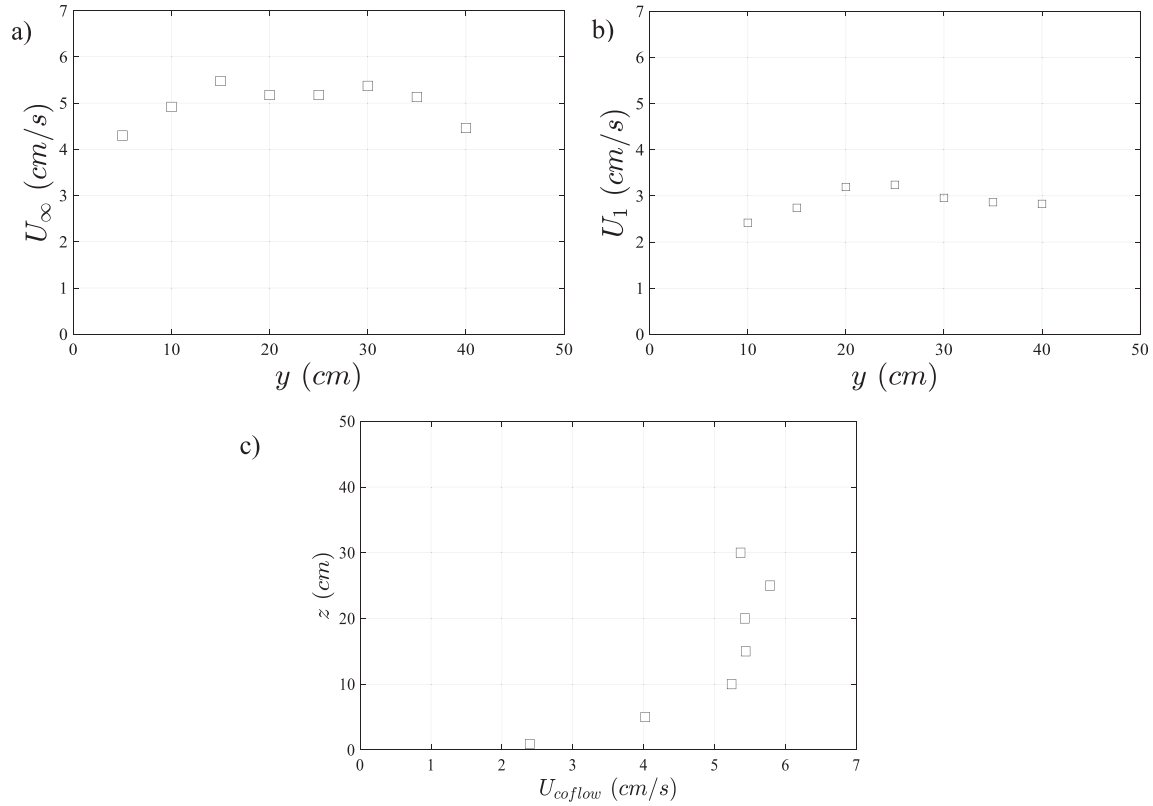


**FIG. 5.** Coflow velocity profiles: (a) lateral profile measured at the mid-depth of the channel, (b) lateral profile measured at $z = z_m$, and (c) vertical profile measured at the mid-width of the channel.

The width of the wall jet in a coflow is also significantly narrower than that in a quiescent background in the lateral direction, whereas the widths of wall jets in coflow and quiescent background are similar in the vertical direction.

Figure 9 plots the normalized lateral profile of $V$ and vertical profiles of $W$ for $\lambda_j = 36$ at $x/D = 30$, 60, and 80, as well as the respective profiles of the wall jet in a quiescent background. It can be seen that the lateral velocities of the wall jet in a coflow are lower than the values for the case with no coflow [Fig. 9(a)]. This indicates that the coflow results in a slower lateral growth of the wall jet. On the other hand, the magnitude of the vertical velocities (for $z/z_{1/2} < 2$) increases, implying that the magnitude of flow toward the wall increases in the presence of the coflowing stream.

Coflowing wall jets grow linearly with the downstream distance in the lateral and vertical directions, similar to the wall jet in a quiescent background. The lateral and vertical spreading rates for various values of $\lambda_j$ are summarized in Table III. It can be seen that the spreading rate of coflowing wall jets (particularly in the lateral direction) is smaller than that of the wall jet in a quiescent background. This result is consistent with the slower decay rates and smaller lateral velocities of coflowing wall jets. Moreover, the spreading rate of wall jets in a coflow increases with increasing $\lambda_j$ and tends to that of wall jets in a quiescent background for very large $\lambda_j$.

**TABLE II.** Coflow statistics.

| Measurement range | $U_\infty$ | $u_{\infty\,rms}$ | $U_1$ | $u_{1\,rms}$ |
|---|---|---|---|---|
| $30 \le x/D \le 100$ | 5.06 cm/s | 0.42 cm/s | 2.80 cm/s | 0.58 cm/s |

The previous results have demonstrated that the mean velocity of coflowing circular wall jets decayed at slower rates, and reached self-similarity farther downstream (i.e., developed more slowly) compared to circular wall jets in a quiescent background. The outward lateral mean velocities and the spreading rate of wall jets in a coflow are also smaller than the case with no coflow. From this, it can be hypothesized that the mass flow rate of wall jets and the entrainment into the wall jets reduce in the presence of coflowing streams. The reduced entrainment and subsequent mixing may be due to (i) the vortical structures of the wall jet, which play a dominant role on the mixing of the flow (Law and Herlina, 2002; Mahmoudi and Fleck, 2017), being suppressed by the coflowing stream; and (ii) the wall jet growth being limited by the wall on one side and the coflow on the other side. Due to the three-dimensional structure of the flow, it is nevertheless difficult to reach a firm conclusion about the effect of a coflow on the entrainment into wall jets and more experimental studies (especially ones in which a scalar concentration field of a jet could be measured) would help to confirm (or refute) this hypothesis.

Figure 10 plots the downstream evolution of the axial RMS velocities measured along the line defined by $(y, z) = (0, z_m)$ (i.e., $u_{m\ rms}$)

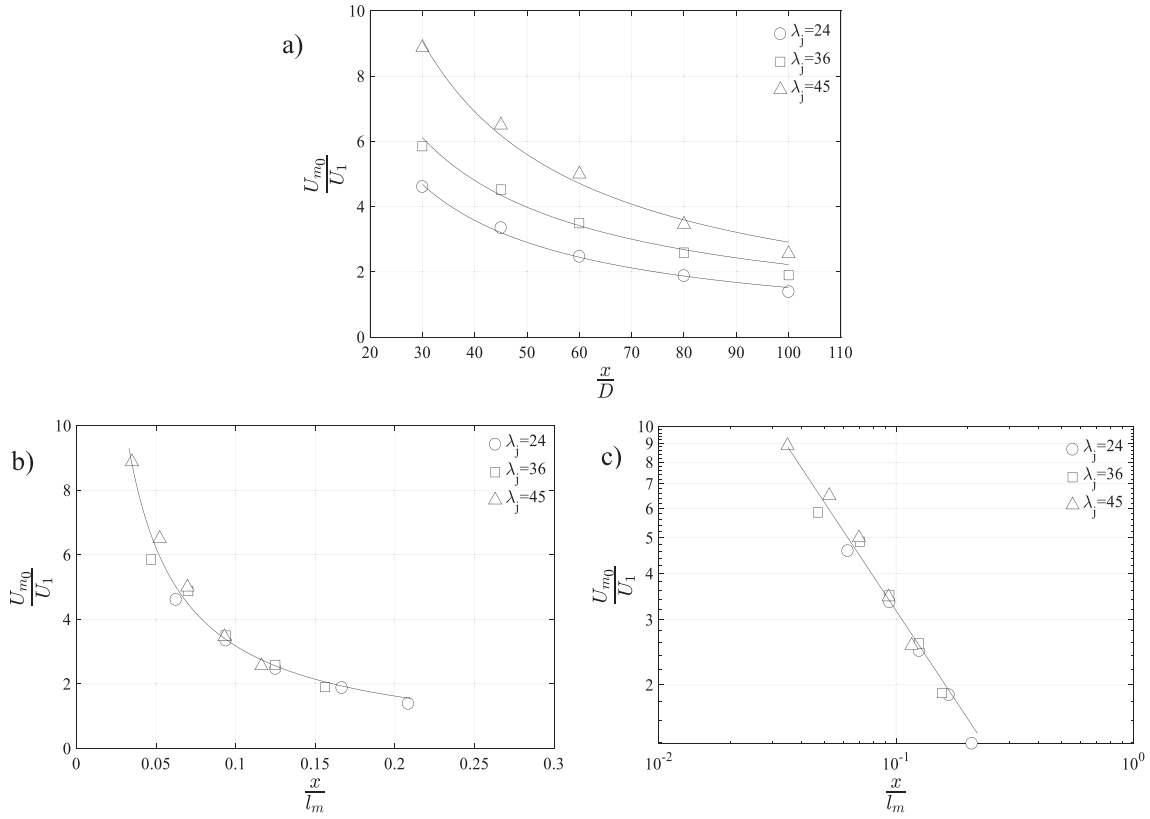


**FIG. 6.** Downstream evolution of the maximum axial mean velocity excess measured for various values of $\lambda_j$ as a function of (a) $x/D$ in linear coordinates; (b) $x/l_m$ in linear coordinates; and (c) $x/l_m$ in log–log coordinates.

normalized by (a) the maximum axial mean excess velocity, and (b) the exit velocity of wall jets (which is constant for each $\lambda_j$), for various values of $\lambda_j$. The RMS velocities of a wall jet in a quiescent background are also presented, for comparison. It can be seen in Fig. 10(a) that the RMS velocities approach an asymptotic value of 0.25 at $x/D \geq 60$. There are also less variations at $x/D \geq 60$ (i.e., in the self-similar region) in the RMS velocities of the wall jets in a coflow compared to those in a quiescent background. As shown in Fig. 10(b), the RMS velocities of coflowing wall jets normalized by $U_j$ are larger than those of the wall jet in a quiescent background in the self-similar region. Note that a reverse trend is observed in Fig. 10(a) due to the higher values of $U_{m_0}$ in coflowing wall jets, which results from their slower decay. Furthermore, the difference between the RMS velocities of coflowing wall jets at various $\lambda_j$ decreases with the downstream distance [see Fig. 10(b)]. At very far downstream distances, where the wall jet becomes weak and its structure is disrupted by the coflow, it is expected that the RMS velocities of wall jets asymptote to that of the coflow.

The lateral and vertical profiles of the axial [Figs. 11(a) and 11(b)], lateral [Figs. 11(c) and 11(d)], and vertical [Figs. 11(e) and 11(f)] RMS velocities, nondimensionalized by the maximum axial mean excess velocity, are plotted for various values of $\lambda_j$ at $x/D = 60$. The lateral profiles are approximately self-similar and independent of $\lambda_j$ particularly close to the jet axis [i.e., $(y, z) = (0, z_m)$], consistent with the observations of the mean velocity profiles. The vertical profiles exhibit self-similarity to a lesser extent than their lateral counterparts.

Figure 12 depicts the lateral and vertical profiles of normalized RMS velocities for $\lambda_j = 36$ at $x/D = 30$, 60, and 80. The data pertaining

**TABLE III.** Decay and spreading rates of coflowing wall jets (compared with those of a wall jet in a quiescent background).

| Study | $\lambda_j$ | Measurement range | $n_0\left[\frac{U_{m_0}}{U_1} = A_0\left(\frac{x}{D}\right)^{-n_0}\right]$ | $\frac{dy_{1/2}}{dx}$ | $\frac{dz_{1/2}}{dx}$ | $\frac{dy_{1/2}}{dx} / \frac{dz_{1/2}}{dx}$ |
|---|---|---|---|---|---|---|
| Coflowing wall jet | 24 | $30 \leq x/D \leq 100$ | 0.98 | 0.17 | 0.03 | 5.6 |
| | 36 | | 1.00 | 0.18 | 0.03 | 6.0 |
| | 45 | | 1.17 | 0.20 | 0.04 | 5.0 |
| Wall jet in a quiescent background | $\infty$ | $30 \leq x/D \leq 110$ | 1.24 | 0.26 | 0.04 | 6.5 |

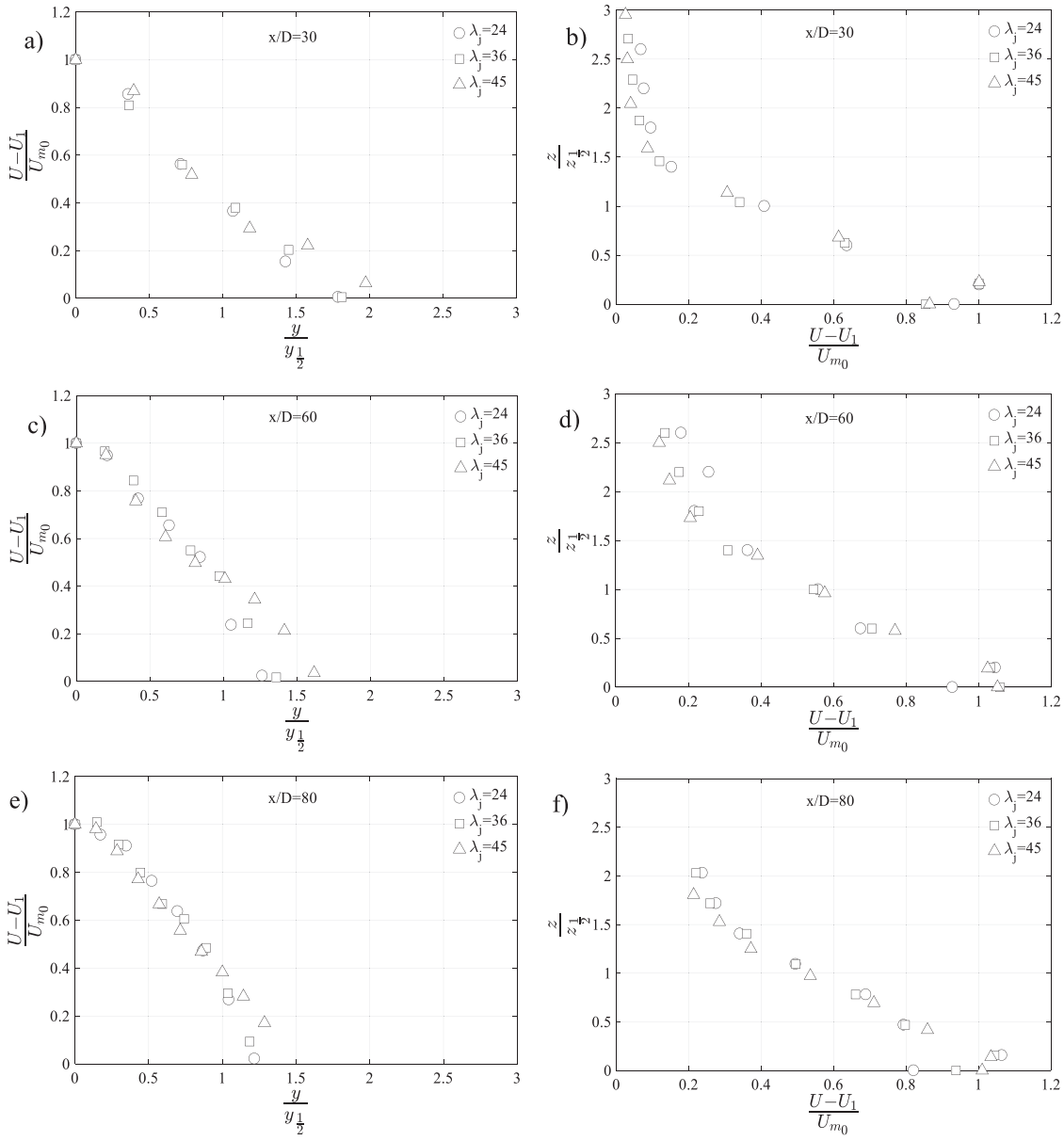


**FIG. 7.** Profiles of the normalized axial mean velocity excess of coflowing jets at various values of $\lambda_j$ plotted along (a) lateral and (b) vertical directions at $x/D = 30$; (c) lateral and (d) vertical directions at $x/D = 60$; and (e) lateral and (f) vertical directions at $x/D = 80$.

to a wall jet in a quiescent background is also presented for comparison. The profiles of the RMS velocities of coflowing wall jets are narrower than those for the wall jet in a quiescent background in the lateral direction, consistent with the observations of the lateral profiles of axial mean velocity in Fig. 8. Furthermore, the profiles are approximately self-similar for $x/D \geq 60$. It is worth noting that self-similarity was not observed in coflowing circular turbulent jets far from boundaries (Antonia and Bilger, 1973; Smith and Hughes, 1977; Moeini *et al.*, 2021) and circular turbulent jets in turbulent backgrounds with zero-mean flow (Khorsandi *et al.*, 2013; Lai *et al.*, 2019). In contrast, the self-similarity of coflowing wall jets might be due to the bounding effect of the wall on one side, which makes the flow more stable than coflowing jets (Mahmoudi and Fleck, 2017). Note that the profiles of RMS velocities of the coflowing jets are higher than those of the quiescent wall jets when normalized by $U_j$ (not shown).

Figure 13 plots the Eulerian temporal power spectra of the axial, lateral, and vertical velocities of wall jets issued into a coflow ($\lambda_j = 36$ and $\mathrm{Re} = 10\,000$) and a quiescent background ($\mathrm{Re} = 10\,000$). The velocity spectra were measured at $(x, y, z) = (60D, 0, z_m)$. The spectra of the wall jets released into the coflow and quiescent background

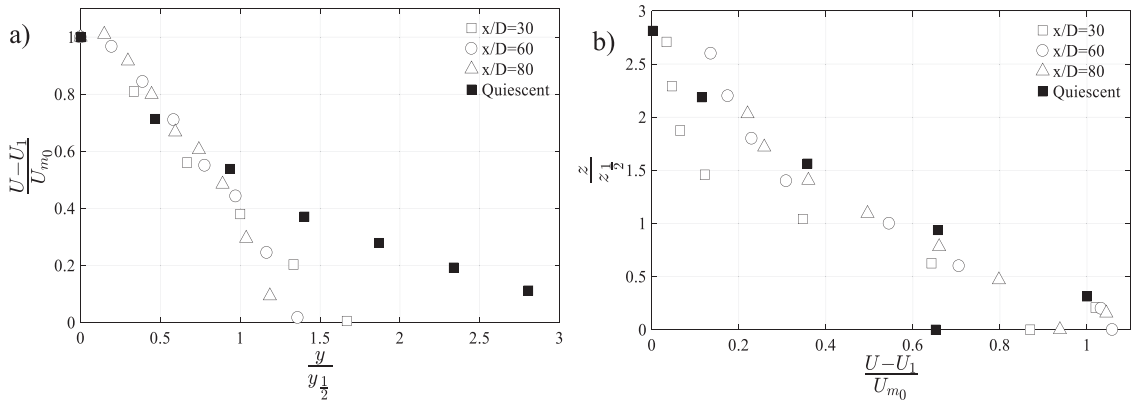


**FIG. 8.** (a) Lateral and (b) vertical profiles of the normalized axial mean velocity excess ($\lambda_j = 36$) at $x/D = 30$, 60, and 80 compared with the self-similar profiles of a wall jet in a quiescent background.

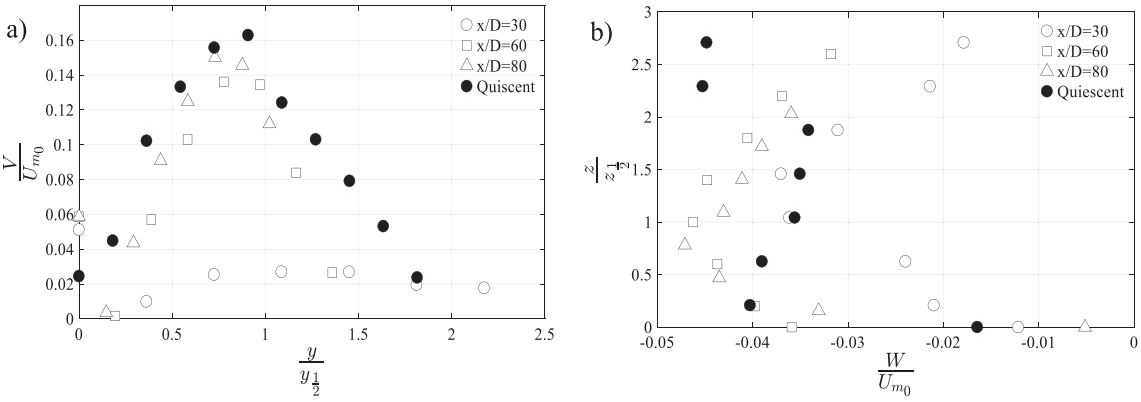


**FIG. 9.** Normalized (a) lateral profile of the lateral mean velocity and (b) vertical profile of the vertical mean velocity ($\lambda_j = 36$) at $x/D = 30$, 60, and 80 compared with the respective profiles of a wall jet in a quiescent background.

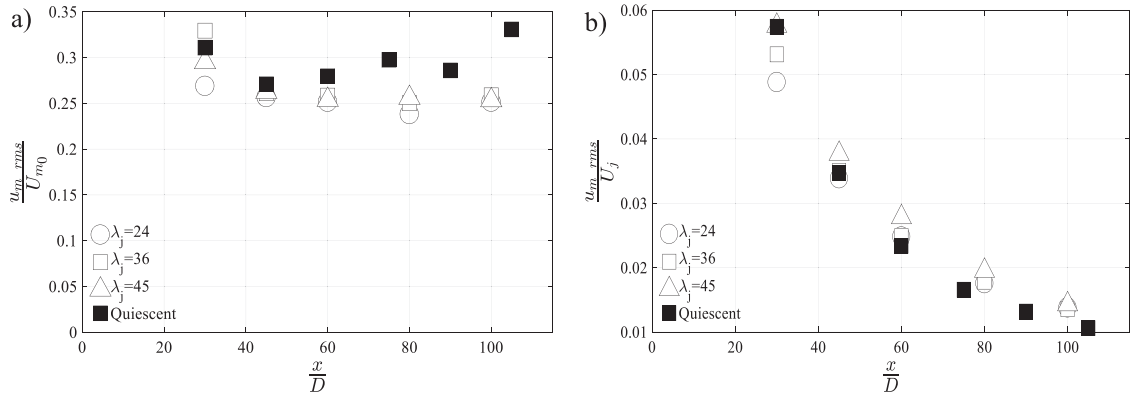


**FIG. 10.** Downstream variations of the axial RMS velocities along the line defined by ($y$, $z$) = (0, $z_m$) normalized by (a) the maximum axial mean excess velocity, and (b) the jet exit velocity, for wall jets released into a coflow and a quiescent background.

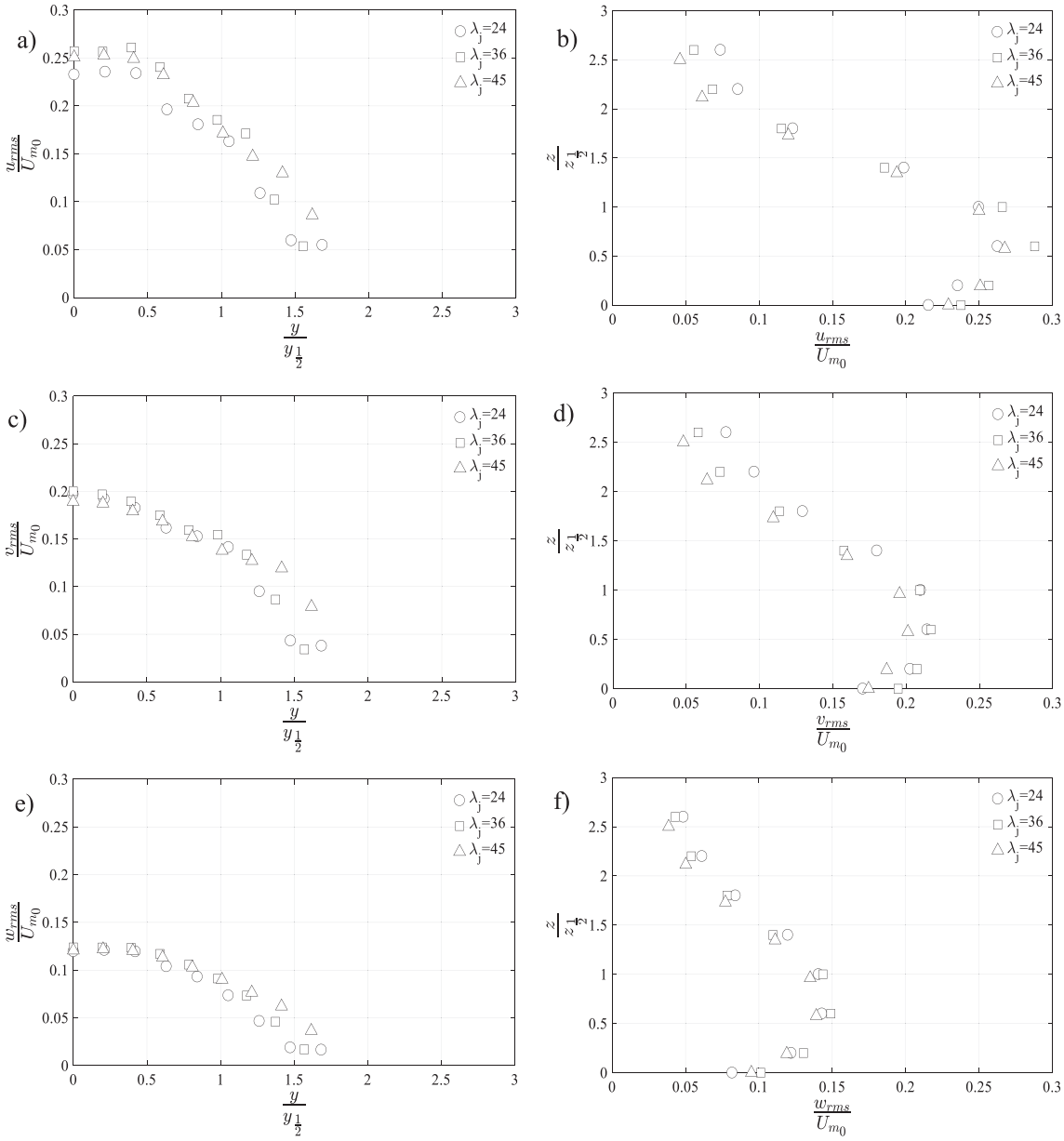


**FIG. 11.** Lateral and vertical profiles of the (a) and (b) axial, (c) and (d) lateral, and (e) and (f) vertical RMS velocities (normalized by the maximum axial mean excess velocity) plotted for various $\lambda_j$ at $x/D = 60$.

have similar shapes and agree reasonably well with the −5/3 power-law spectrum in the inertial subrange, although the slope of the axial and lateral velocity spectra are somewhat shallower than that of the vertical velocity. The spectra of the coflowing wall jets have slightly higher values compared to those of the wall jet in a quiescent background. This is consistent with the observed relatively high values of the RMS velocities in coflowing wall jets. (Recall that the square of RMS velocities, i.e., the velocity variance, is equal to the area under the spectra.) As observed in the spectra, all large-scale quantities are well resolved, indicating that the 25-Hz sampling frequency of the ADV was sufficiently high to accurately measure large-scale turbulence quantities, such as the RMS velocities.

## IV. CONCLUSIONS

The three-dimensional velocity field of circular turbulent wall jets issued into both quiescent surroundings and a coflow was measured. Profiles of the statistics of the three velocity components in the three directions were presented. The mean and RMS velocity fields of the wall jet issued into a quiescent background agreed well with those measured in past studies. The results showed that the coflow restricts

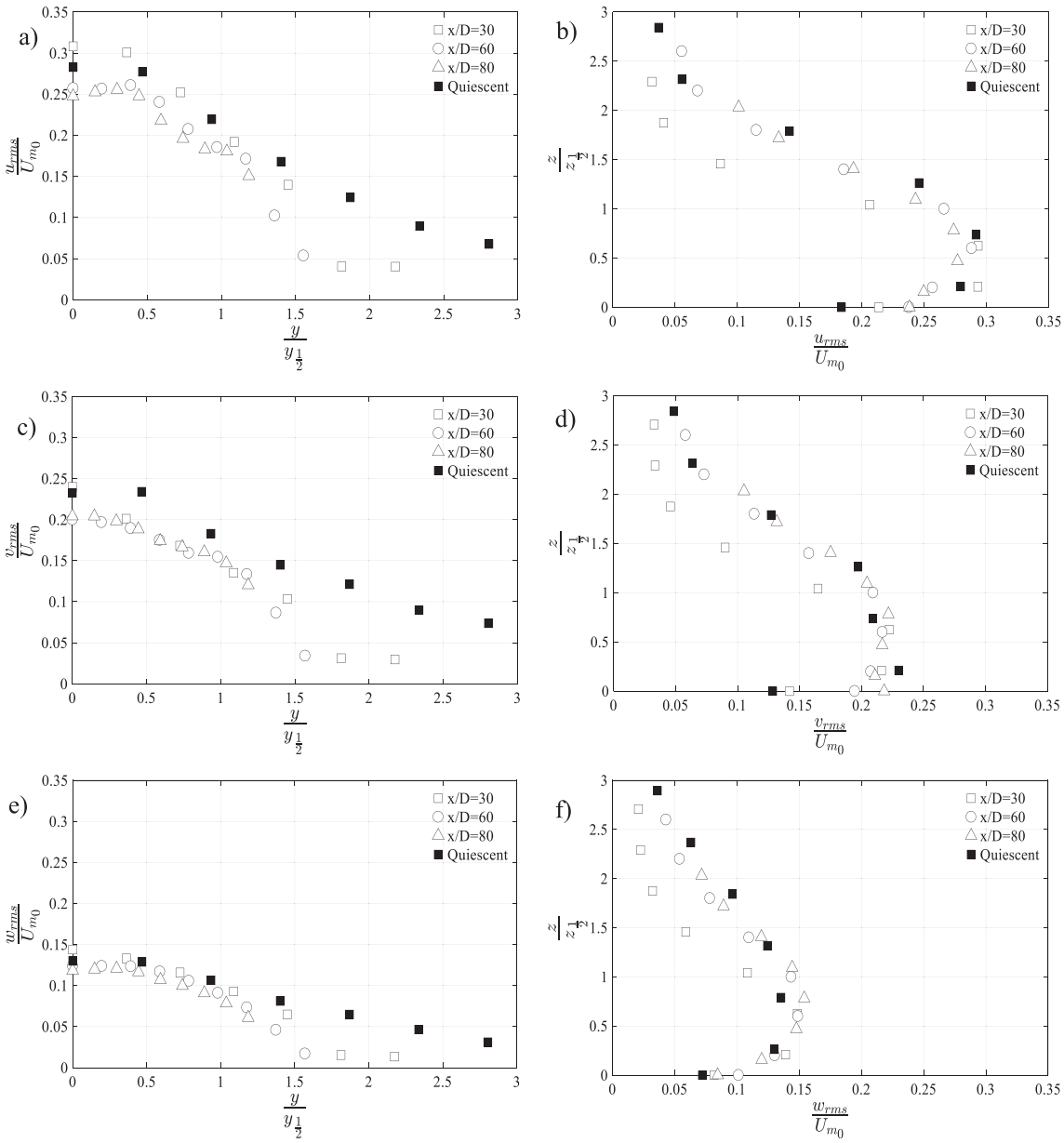


**FIG. 12.** Lateral and vertical profiles of the (a) and (b) axial, (c) and (d) lateral, and (e) and (f) vertical RMS velocities (normalized by the maximum axial mean excess velocity) plotted for $\lambda_j = 36$ and various downstream distances.

the wall jet's growth and delays its development. It was observed that the decay rate, spreading rate, and the outward mean lateral velocities of the wall jets are reduced in the presence of a coflow. The decay and spreading rates were found to increase as the jet-to-coflow velocity ratio increased and tended to those of a wall jet in a quiescent background as the ratio increased to infinity. From the slower decay, narrower width, and smaller magnitude of lateral velocities of coflowing wall jets, it was hypothesized that a coflow results in a decrease in the mass flow rate of wall jets. Therefore, the entrainment into the wall jet and the subsequent mixing with the ambient fluid reduces, presumably due to the suppression by the coflow of the wall jet vortical structures. Both the mean and RMS velocities of coflowing wall jets were found to be nearly self-similar, although the onset of the self-similarity was delayed to farther downstream distances relative to the wall jet in a quiescent background. The self-similarity of the RMS velocities of coflowing wall jets was contrasted with the observations in coflowing jets in previous studies. The velocity spectra of walls jets issued into a quiescent background and coflowing stream were observed to be similar in shape (for each measurement direction). However, the latter had higher values, consistent with the observed trends for the RMS velocities. Finally,

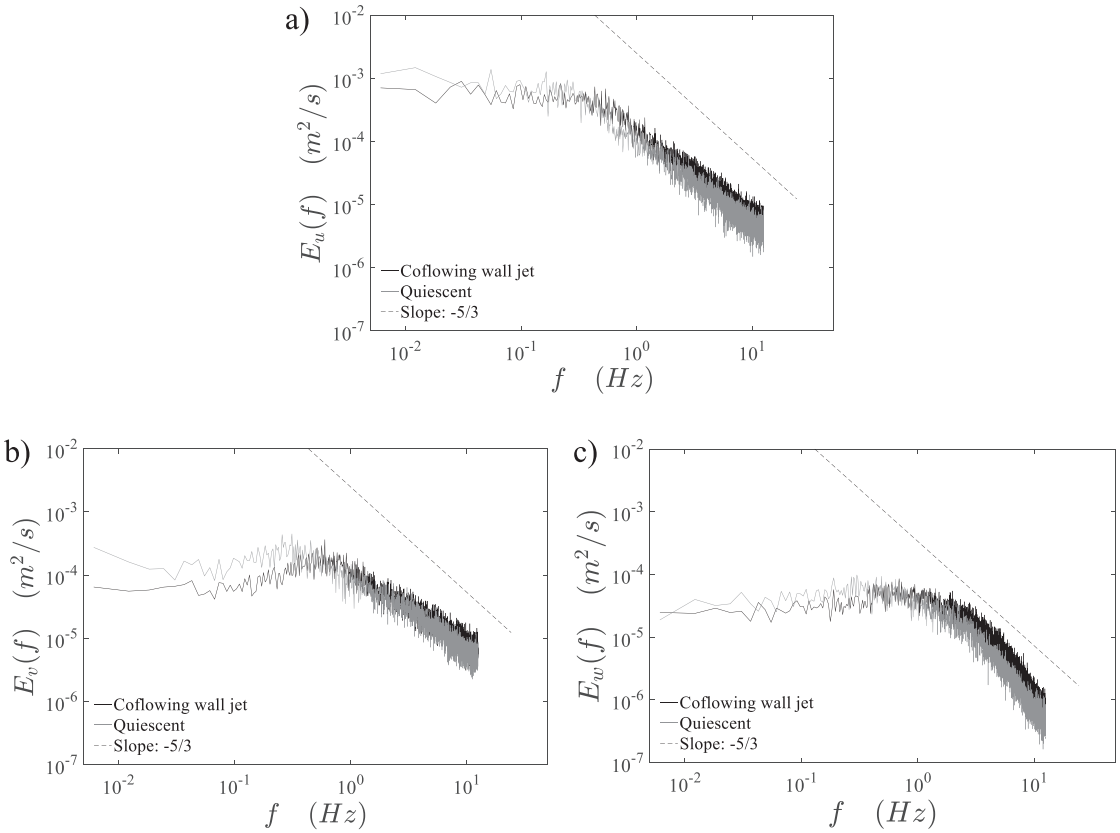


**FIG. 13.** (a) Axial ($u$), (b) lateral ($v$), and (c) vertical ($w$) velocity spectra measured at the jet centerline at $x/D = 60$ for a jet released into a quiescent background and coflow.

for future studies, we recommend conducting (i) velocity measurements with relatively high coflow velocities (i.e., lower jet-to-coflow velocity ratios), to examine the dynamics and mixing of weaker coflowing wall jets, and (ii) scalar measurements to more accurately quantify entrainment and mixing of wall jets in a coflow.

## ACKNOWLEDGMENTS

The authors would like to thank the Natural Sciences and Engineering Research Council (NSERC) of Canada for funding part of this work (Grant No. RGPIN-2018-05848 to L.M.).

## AUTHOR DECLARATIONS

### Conflict of Interest

The authors have no conflicts to disclose.

## DATA AVAILABILITY

The data that support the findings of this study are available from the corresponding author upon reasonable request.

## REFERENCES

Abrahamsson, H., Johansson, B., and Löfdahl, L., "The turbulence field of a fully developed three-dimensional wall jet," Internal Report No. 97/1 (Department of Thermo and Fluid Dynamics, Chalmers Univ. of Tech., Göteborg, Sweden, 1997).

Agelin-Chaab, M., and Tachie, M. F., "Characteristics of turbulent three-dimensional wall jets," J. Fluids Eng. **133**(2), 021201 (2011).

Antonia, R. A., and Bilger, R. W., "An experimental investigation of an axisymmetric jet in a co-flowing air stream," J. Fluid Mech. **61**(4), 805–822 (1973).

Azimi, A. H., Qian, Y., Zhu, D. Z., and Rajaratnam, N., "An experimental study of circular sand–water wall jets," Int. J. Multiphase Flow **74**, 34–44 (2015).

Azimi, A. H., Zhu, D. Z., and Rajaratnam, N., "Experimental study of subaqueous sand deposition from slurry wall jets," J. Eng. Mech. **140**(2), 296–314 (2014).

Chokhar, I. A., Dyachenko, A. Y., Pakhomov, M. A., Philippov, M. V., and Terekhov, V. I., "Experimental study of the effect of a transverse trench depth on film cooling effectiveness," Case Stud. Therm. Eng. **25**, 100934 (2021).

Chu, P. C., Lee, J. H., and Chu, V. H., "Spreading of turbulent round jet in coflow," J. Hydraul. Eng. **125**(2), 193–204 (1999).

Davis, M. R., and Winarto, H., "Jet diffusion from a circular nozzle above a solid plane," J. Fluid Mech. **101**(1), 201–221 (1980).

Dey, S., Kishore, G., Castro-Orgaz, O., and Ali, S. Z., "Hydrodynamics of submerged turbulent plane offset jets," Phys. Fluids **29**, 065112 (2017).

Godi, S. C., Pattamatta, A., and Balaji, C., "Effect of the inlet geometry on the flow and heat transfer characteristics of three-dimensional wall jets," J. Heat Transfer **141**(11), 112201 (2019).

Goring, D. G., and Nikora, V. I., "Despiking acoustic Doppler velocimeter data," J. Hydraul. Eng. **128**(1), 117–126 (2002).

Hussein, H. J., Capp, S. P., and George, W. K., "Velocity measurements in a high-Reynolds-number, momentum-conserving, axisymmetric, turbulent jet," J. Fluid Mech. **258**, 31–75 (1994).

Ji, Y., Yao, J., Hussain, F., and Chen, X., "Vorticity transports in turbulent channels under large-scale control via spanwise wall jet forcing," Phys. Fluids **33**, 095112 (2021).

Kakka, P., and Anupindi, K., "Flow and thermal characteristics of three-dimensional turbulent wall jet," Phys. Fluids **33**, 025108 (2021).
Kazemi, M., Khorsandi, B., and Mydlarski, L., "Effect of acoustic Doppler velocimeter sampling volume size on measurements of turbulence," J. Atmos. Ocean Technol. **38**(2), 259–268 (2021).
Khorsandi, B., Gaskin, S., and Mydlarski, L., "Effect of background turbulence on an axisymmetric turbulent jet," J. Fluid Mech. **736**, 250–286 (2013).
Khorsandi, B., Mydlarski, L., and Gaskin, S., "Noise in turbulence measurements using acoustic Doppler velocimetry," J. Hydraul. Eng. **138**(10), 829–838 (2012).
Lai, A., Law, A., and Adams, E., "A second-order integral model for buoyant jets with background homogeneous and isotropic turbulence," J. Fluid Mech. **871**, 271–304 (2019).
Launder, B. E., and Rodi, W., "The turbulent wall jet measurements and modeling," Annu. Rev. Fluid Mech. **15**(1), 429–459 (1983).
Law, A. W.-K., and Herlina, "An experimental study on turbulent circular wall jets," J. Hydraul. Eng. **128**(2), 161–174 (2002).
Li, Z., and Huai, W., "Turbulence characteristics of a round offset jet with different offset ratios in a counterflow," Environ. Fluid Mech. **20**(4), 689–706 (2020).
Mahmoudi, M., and Fleck, B. A., "Experimental measurement of the velocity field of round wall jet in counterflow," J. Hydraul. Eng. **143**(1), 04016076 (2017).
Moeini, M., Khorsandi, B., and Mydlarski, L., "Effect of acoustic Doppler velocimetry sampling frequency on statistical measurements of turbulent axisymmetric jets," J. Hydraul. Eng. **146**(7), 04020048 (2020).
Moeini, M., Khorsandi, B., and Mydlarski, L., "Effect of coflow turbulence on the dynamics and mixing of a non-buoyant turbulent jet," J. Hydraul. Eng. **147**(1), 04020088 (2021).
Nejatipour, P., and Khorsandi, B., "Effect of nozzle geometry on the dynamics and mixing of self-similar turbulent jets," Water Sci. Technol. **84**(12), 3907–3915 (2021).
Nickels, T. B., and Perry, A. E., "An experimental and theoretical study of the turbulent coflowing jet," J. Fluid Mech. **309**, 157–182 (1996).
Nortek, *The Comprehensive Manual for Velocimeters* (Nortek, 2018).
Nyantekyi-Kwakye, B., Tachie, M. F., Clark, S. P., Malenchak, J., and Muluye, G. Y., "Experimental study of the flow structures of 3D turbulent offset jets," J. Hydraul. Res. **53**(6), 773–786 (2015).
Or, C. M., Lam, K. M., and Liu, P., "Potential core lengths of round jets in stagnant and moving environments," J. Hydro-environ. Res. **5**(2), 81–91 (2011).
Padmanabham, G., and Lakshmana Gowda, B. H., "Mean and turbulence characteristics of a class of three-dimensional wall jets—Part 1: Mean flow characteristics," J. Fluids Eng. **113**(4), 620–628 (1991).
Sforza, P. M., and Herbst, G., "A study of three-dimensional, incompressible, turbulent wall jets," AIAA J. **8**(2), 276–283 (1970).
Sharma, S., Jesudhas, V., Balachandar, R., and Barron, R., "Turbulence structure of a counter-flowing wall jet," Phys. Fluids **31**, 025110 (2019).
Shojaeizadeh, A., Safaei, M. R., Alrashed, A. A., Ghodsian, M., Geza, M., and Abbassi, M. A., "Bed roughness effects on characteristics of turbulent confined wall jets," Measurements **122**, 325–338 (2018).
Smith, D., and Hughes, T., "Some measurements in a turbulent circular jet in the presence of a co-flowing free stream," Aeronaut. Q. **28**(3), 185–196 (1977).
Sun, H., and Ewing, D., "Effect of initial and boundary conditions on development of three-dimensional wall jets," in *40th AIAA Aerospace Sciences Meeting & Exhibit* (AIAA, 2002), p. 733.
Wahl, T. L., "Discussion of 'Despiking acoustic Doppler velocimeter data' by Derek G. Goring and Vladimir I. Nikora," J. Hydraul. Eng. **129**(6), 484–487 (2003).
Xu, K., Ren, Y., and Zha, G., "Separation control by co-flow wall jet," in *AIAA AVIATION 2021 FORUM* (AIAA, 2021), p. 2946.
Zhang, Z., Guo, Y., Zeng, J., and Zheng, J., "Numerical simulation of vertical buoyant wall jet discharged into a linearly stratified environment," J. Hydraul. Eng. **144**(7), 06018009 (2018).